To Stop or to Shuttle Halides? The Role of an Ionic Liquid in Thermal Halide Mixing of Hybrid Perovskites

Christopher Greve, Philipp Ramming, Markus Griesbach, Nico Leupold, Ralf Moos, Anna Köhler, Eva M Herzig, Fabian Panzer, Helen Grüninger

To Stop or to Shuttle Halides? The Role of an Ionic Liquid in Thermal Halide Mixing of Hybrid Perovskites

Christopher Greve,[1#] Philipp Ramming,[2#] Markus Griesbach,[2] Nico Leupold,[3] Ralf Moos,[3] Anna Köhler,[2] Eva M. Herzig,[1] Fabian Panzer,[2] Helen Grüninger[4]*

[1] Herzig Group - Dynamics and Structure Formation, University of Bayreuth, 95440 Bayreuth, Germany.

[2] Soft Matter Optoelectronics, University of Bayreuth, 95440 Bayreuth, Germany.

[3] Department of Functional Materials, University of Bayreuth, 95440 Bayreuth, Germany.

[4] Inorganic Chemistry III, University of Bayreuth, 95440 Bayreuth, Germany.

# These authors contributed equally

*Correspondence to: helen.grueninger@uni-bayreuth.de

ORCID IDs

Helen Grüninger: 0000-0002-5422-7003

Fabian Panzer: 0000-0002-2191-9011

Eva M. Herzig: 0000-0002-0151-5562

Anna Köhler: 0000-0001-5029-4420

Ralf Moos: 0000-0001-7622-0120

Christopher Greve: 0000-0001-5506-9695

Abstract

Ionic liquids, like $BMIMBF_4$, are added to mixed halide perovskites to prevent halide phase segregation and increase phase stability, but exact mechanisms changing halide kinetics are currently unclear. Here, X-ray diffraction, nuclear magnetic resonance and photoluminescence spectroscopy are used *in-situ* under dark conditions to follow thermally driven halide mixing processes forming $MAPbI_{3-x}Br_x$ from physical mixtures of $MAPbI_3$ and $MAPbBr_3$ powders with and without $BMIMBF_4$. Halide migration is significantly accelerated with $BMIMBF_4$ compared to additive-free mixtures. This is attributed to liquid-like dynamics of $BMIMBF_4$ at elevated temperatures, liberating defect sites at perovskite interfaces. Furthermore, the presence of $BMIMBF_4$ increases the activation energies for Bromide migration, suggesting a changed nature of the latter. This is explained by a preferred interaction between $BMIM^+$ and Bromide, indicating that the cations of the additive shuttle Bromide ions between interfaces. Overall, these observations pave the way for a better understanding of halide transport in hybrid perovskites.

TOC Graphic

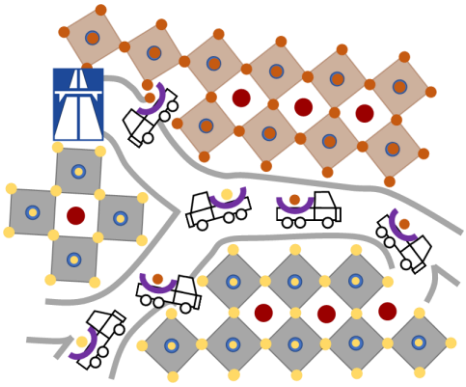

Main text

In recent years mixed halide perovskites have become a promising candidate for application in tandem solar cells due to the tunability of their bandgap energy [1,2]. However, in polycrystalline perovskite thin films, halide migration within perovskite grains and across their interfaces results in phase segregation of halides under light irradiation and thus in a deterioration of optoelectronic functionality [3–6]. Therefore, major efforts were undertaken to study halide diffusion, the driving force behind the halide demixing processes under external stimuli, such as light irradiation[3,7,8], electrical bias [9,10] and heat treatment [11–13]. The various studies revealed that illumination-induced halide segregation i) depends on the light intensity and temperature,[11,13,14] ii) mainly appears at grain boundaries [15] and iii) is reversible in the dark [3,11]. This reversal of the halide mixing process is accelerated through annealing and results in solid solutions, e.g., in the case of the often studied mixed halide perovskite $MAPbI_{3-x}Br_x$.[16] The corresponding halide mixing and demixing reaction is described by Eq. 1 in a simplified manner, whereby the formation of intermediate halide compositions is indicated. Phase segregation under illumination usually is reaching a stable plateau for x around 0.6 for Iodide rich composition, while Bromide rich compositions are less stable and highly distributed. [3,17]

$$MAPbI_3 + MAPbBr_3 \xrightarrow{\Delta T} MAPbI_{3-x}Br_x + MAPbI_xBr_{3-x} \underset{h\nu}{\overset{\Delta T}{\rightleftarrows}} 2\,MAPbI_{1.5}Br_{1.5} \qquad \text{Eq.1}$$

In general, halide diffusion in halide perovskites, and therefore also halide segregation or mixing (Eq. 1), is defect-assisted[7,16] via bulk and surface ionic defects.[18,19] Consequently, the underlying mechanism of ion migration can vary with the chosen halide composition,[20] as well as the overall perovskite morphology. This leads to a high variation of extracted activation energies for Iodide and Bromide migration, ranging

between 7.7 kJ/mol and 57.9 kJ/mol (0.08 eV - 0.6 eV).[11,14,18,21,22] It was also shown that in thin films of mixed $MAPbI_{1.5}Br_{1.5}$, the activation energies for remixing are higher than for light-induced segregation,[11] which was correlated to lattice expansion and strain due to the presence of charge carriers under illumination.[23,24]

One approach to inhibit ion migration and thus counter halide segregation upon illumination is the use of additives. Additives reduce bulk defect densities [15,22] and modify interfaces in perovskite thin films, [25–27] hindering ion migration. Here, one prominent type of additive are ionic liquids (ILs). ILs are known to improve the stability of halide perovskites against humidity,[28,29] facilitate film processing,[30,31] foster grain growth,[32,33] and passivate trap states[34–36]. Amongst a suit of different ILs, especially ILs with an imidazolium-based cation are widely used for defect passivation, as well as performance and stability enhancements.[37–39] It was demonstrated that the imidazolium core of the cation governs the functionality for a range of different side groups, while the nature of the associated anion, e.g., halides or super halogens, is modulating the observed effects for a variety of hybrid perovskite compositions.[38,40,41] More specifically, the imidazolium-based super halogen IL $BMIMBF_4$ (1-Butyl-3-methylimidazolium tetrafluoroborate) was used to enhance the thermal stability in $MAPbI_3$ and mixed halide perovskite thin film solar cells under light irradiation and to suppress the ion migration in $MAPbI_3$ powder thick films.[36,42,43] However, what role the IL plays for halide migration and how it interacts with the perovskite is still rather unclear.[44] To this end, we investigate how the additive $BMIMBF_4$ impacts halide diffusion in the reversed process to demixing, i.e. the halide mixing in perovskites upon annealing (Eq. 1).

We study the halide migration kinetics during thermally induced halide mixing in physical mixtures (1:1) of $MAPbI_3$ and $MAPbBr_3$ powders with $BMIMBF_4$ as additive

under dark conditions. For this, the neat “parent” perovskite powders $MAPbI_3$ and $MAPbBr_3$ were individually synthesized using a mechanochemical approach,[45] with and without the addition of 0.5 mol% $BMIMBF_4$ during ball-milling (compare SI, section S1 for details). To identify if the functionality of $BMIMBF_4$ is based on the cation or anion a further set of parent powders is synthesized containing 0.5 mol% $BMIMPF_6$ (see section S1). The resulting $MAPbI_3$ and $MAPbBr_3$ powders with and without ILs possess similar powder morphologies, i.e., particle size, crystallinity, and bulk defect densities, as analyzed by SEM, XRD, NQR and PL spectroscopy (details in section S2 in SI). Consequently, changes in halide kinetics should be attributed to the presence of $BMIMBF_4$ and $BMIMPF_6$ located at grain boundaries.[43,46] Furthermore, the mean grain pseudoradii around 0.2 µm suggest that the halide migration is dominated via the modified grain boundaries.[47]

The $MAPbI_3$ and $MAPbBr_3$ powders are physically mixed (1:1) by cryo-ball milling at low temperature (T=77 K) to ensure well dispersed, reproducible particle interface contacts and at the same time to avoid halide mixing at this stage. The halide mixing process in the physical $MAPbI_3$:$MAPbBr_3$ mixtures is then stimulated by heating to different temperatures between 55°C and 90°C, and monitored *in-situ* by XRD, ^{207}Pb NMR and PL spectroscopy (see SI, section S1 for method protocol). The ^{207}Pb NMR chemical shifts are sensitive to the composition of halides in the local environment and as such to the first octahedral halide coordination shell.[48] NMR spectroscopy generally is a bulk method that provides an average image sensitive to the bulk and surface of the powder, while XRD provides information on the overall phase distribution of perovskite phases in the bulk. PL is highly sensitive to low-energy emitting sites, due to charge carrier funneling into I-rich domains with lower bandgap.[24,49] Thus, PL allows to primarily probe I-rich domains.[17,24] Due to the strong absorption in metal halide

perovskites, most excited states are present within the first ~ 300 nm, making PL particularly surface sensitive.

Exemplarily, Figure 1 shows the NMR and PL spectra and XRD patterns at the beginning and after 1340 min of applying 90°C in the dark to a 1:1 $MAPbI_3$:$MAPbBr_3$ powder mixture containing $BMIMBF_4$. The initial ^{207}Pb NMR spectrum (Figure 1A, orange) shows two distinct signals at chemical shifts of δ = 1450 ppm and 400 ppm, which are typical for lead in pure octahedral I^- coordination and Br^- coordination, i.e., physically mixed $MAPbI_3$ and $MAPbBr_3$.[48,50,51] After 1340 min at 90°C, the final NMR spectrum (black) changes to a broad, but structured intensity distribution located around δ = 1050 ppm. This distribution located between the PbI_6 and $PbBr_6$ signals provides evidence that a mixed perovskite phase evolved, in which various $PbI_{6-x}Br_x$ (x=0, ..., 6) halide coordinations are present.[48] The initial PL spectrum (orange) and that after mixing at 90°C for 1341 min (black) is shown in Figure 1B. The initial PL spectrum consists of two PL peaks at 780 nm and 550 nm, corresponding to pure phases of $MAPbI_3$ and $MAPbBr_3$, respectively.[49] Due to charge carrier funneling from the high band gap $MAPbBr_3$ phase to low band gap $MAPbI_3$ phase the PL peak that corresponds to $MAPbI_3$ is more intense than that of $MAPbBr_3$ despite equal phase ratios.[6,17,49,52] The PL spectrum after t=1341 min displays one peak at 735 nm (Figure 1B). Continuation of the measurement up to 2750 min leads to a further peak shift to 718 nm, which is still far from the expected wavelength for fully mixed $MAPbI_{1.5}Br_{1.5}$ at 683 nm (see Figure S17). Evidently, the observed wavelength of 718 nm after 2750 min indicates that the mixing is not fully completed and some I-rich domains still exist, which dominate the PL emission due to charge carrier funneling.[17]

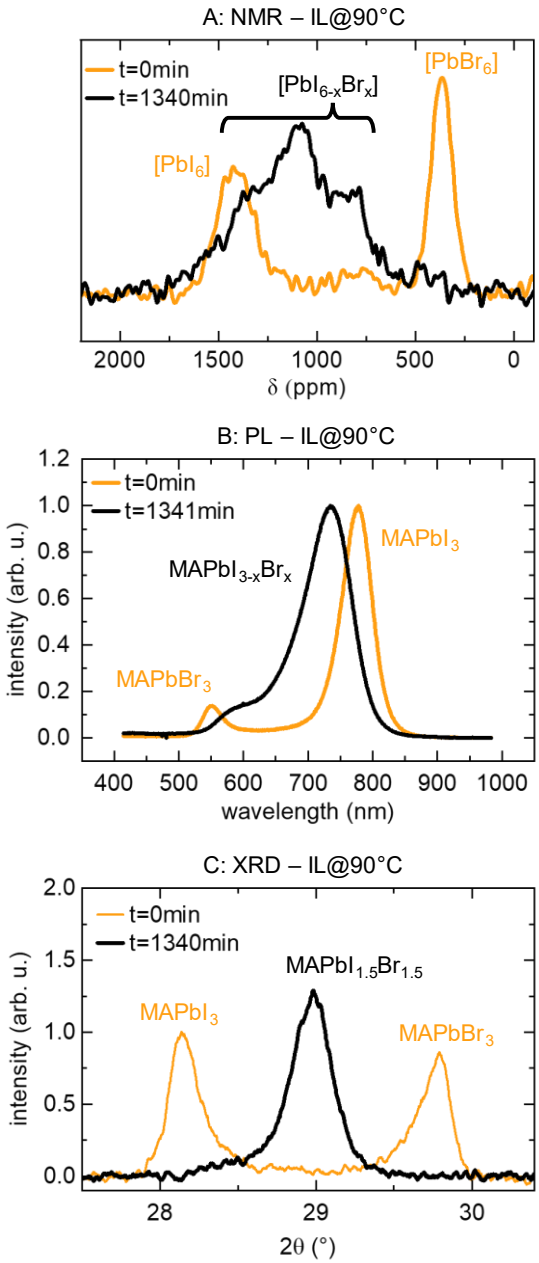

Figure 1: ^{207}Pb NMR and PL spectra and XRD patterns of a physical 1:1 mixture of $MAPbI_3$:$MAPbBr_3$ powders with $BMIMBF_4$ before (orange) and after (black) mixing in the dark at 90°C under inert atmosphere. (A) ^{207}Pb NMR of an initial (binary) powder sample at RT (orange) and final (mixed) sample after 1340 min at 90°C (black). (B) Initial PL spectra of binary sample after reaching 90°C (orange) and mixed sample after 1341 min at 90°C (black). (C) Initial XRD pattern of binary sample after reaching 90°C (orange) and final mixed sample after 1340 min at 90°C (black). The labels indicate the assignment of peak positions to pure or mixed phases.

The initial XRD pattern (orange) measured at 90°C in Figure 1C shows two reflections attributed to (200) scattering of cubic $MAPbI_3$ at 2θ = 28.2° and (200) scattering of cubic $MAPbBr_3$ located at 2θ = 29.7°.[53,54] The slight asymmetric shape of both reflexes indicates the onset of the halide mixing process. After 1340 min at 90°C, the pattern (black) shows a single reflection attributed to a fully mixed $MAPbBr_{1.5}I_{1.5}$ phase,[55] while the initially observed reflections vanished. Longer retention at 90°C only results in a narrowing of the reflection (Figure S14 C) indicating increasing crystallite sizes and/or decreasing strain through annealing.

To assess the halide mixing kinetics, the temporal evolution of the signals from NMR, XRD and PL were followed via fitting the experimental data to extract the specific signal integrals associated to different material compositions from the full spectra and patterns (details see Section 3 SI). For NMR spectra, we focused on the temporal decay in amplitude of the $PbBr_6$ signal, which is well resolved also for mixed perovskite phases. In the XRD patterns we focused on the decays of reflection intensities corresponding to $MAPbI_3$ and $MAPbBr_3$ phases and in the PL spectra on the evolution of the $MAPbI_3$ phase-associated intensity (Figure 2, Figures S7-S9, S13-S19). In this way, we can access both the Bromide and the Iodide migration from the initial binary parent phases into mixed perovskite phases, both locally (NMR and PL) and globally (XRD).

From Figures 2A and 2C, it becomes clear that the decay curves dominantly associated wih Br^- migration, i.e., the $PbBr_6$ NMR and the $MAPbBr_3$ XRD peak decays, are qualitatively comparable for halide mixing at 90°C, for both IL and reference samples (for other temperatures see Figures S20 and S22). The $PbBr_6$ NMR signal does not only originate from pure $MAPbBr_3$, but also from Br-rich mixed $MAPbI_{3-x}Br_x$ phases (x>1.5) that form during heating (Figure S12). Therefore, the experimentally

observed decay of the $PbBr_6$ NMR signal is expected to be slightly flatter than the decay of the pure parent $MAPbBr_3$ phase.

Differences also arise for decay curves dominated by I^- migration (Figure 2B,2D): The XRD patterns and associated decay curves suggest the depletion of the long-range ordered pure phases to be already finished (on average). However, the decays of the PL signals are significantly slower than the corresponding decay curves from XRD (for other temperatures see Figures S22 and S25). This indicates that on the local scale, small I-rich domains may decay more slowly. Charge carrier funnelling, also from formed mixed halide phases, will further enhance the relative proportion of I-rich domains.

Most notably, a significantly faster mixing process is evident for the mixtures with IL (red) compared to the reference mixture (black) for all methods. Especially, the Br^- kinetics tracked by NMR and XRD (Figure 2A, 2C) are strongly accelerated when $BMIMBF_4$ is present, while the increase in I^- mixing kinetics is more moderate (Figure 2B, 2D). This implies that the Br^- transport is more profoundly impacted by the presence of the IL $BMIMBF_4$.

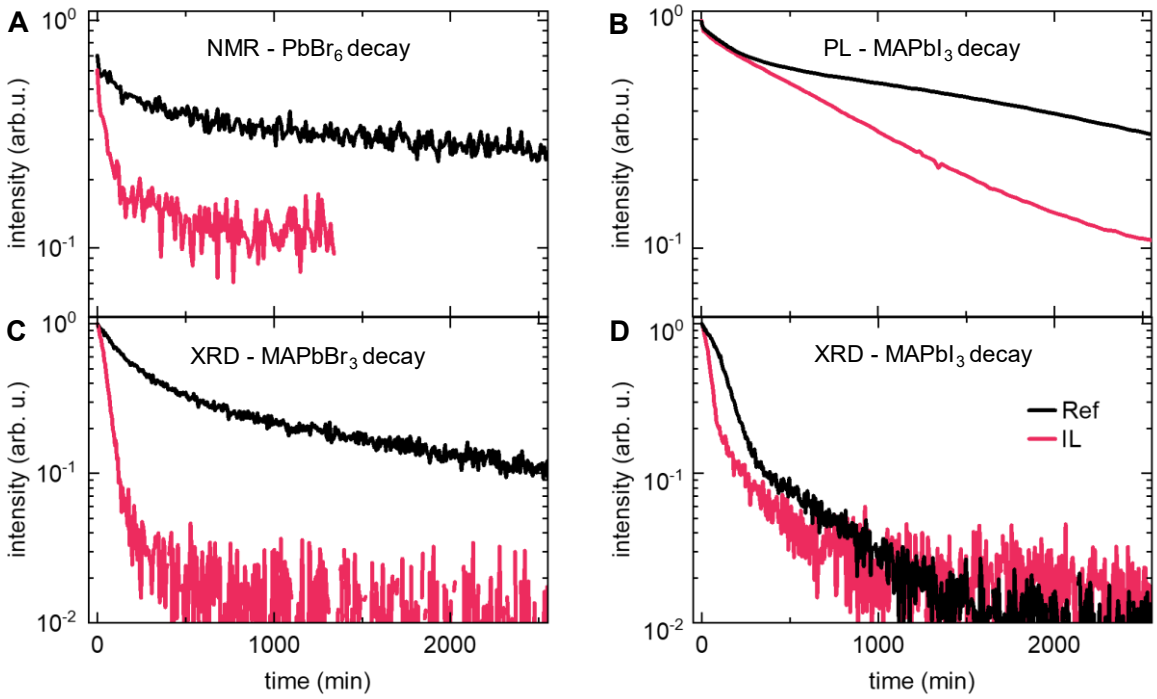

Figure 2: Normalized intensity decay of (A) the resonance of $PbBr_6$ coordination in ^{207}Pb NMR spectra, (B) the $MAPbI_3$ emission in PL spectra, (C) the cubic (200) $MAPbBr_3$ reflection and (D) the cubic (200) $MAPbI_3$ reflection in XRD patterns during thermally induced halide mixing at 90°C between physical $MAPbI_3$:$MAPbBr_3$ powder mixtures (1:1). The label IL denotes the $BMIMBF_4$ containing mixture, while Ref indicates the data obtained from reference perovskite powders that were synthesized without any IL.

For all decay curves, we identify complex halide kinetics (Figure 2, section S4), which consist of an initial fast decay, followed by a slower decay in intensity, with the transition between both decay regimes being earlier for the IL sample. These fast and slow decay regimes appear as linear slopes in the semilogarithmic plots,[56] which indicates that at least two first-order processes are present during the mixing process. The observed halide kinetics with a change from a fast to a slow decay may be attributed to a superposition of several processes influencing the halide migration. These processes might include: I) halide migration in the crystalline bulk and at

interfaces,[47,57] II) dynamic changes of the defect landscape (ion migration pathways) during annealing,[16,47] III) crystal growth and dynamic changes of the compositional gradient,[47,58] which acts as driving force for the configurational entropy gain during the formation of a solid solution or IV) the formation of highly stable Iodide-rich intermediate solid solutions with Bromide contents below 20%.[3,17] Currently, this complex interplay on the halide diffusion is unclear and its disentanglement into a detailed diffusion model exceeds the scope of this study but will be subject of future investigations.

Therefore, despite of the complex interlocking effects on halide kinetics, we describe the kinetic curves by the simplest possible fit to further analyze the effect of $BMIMBF_4$ on thermally induced halide mixing. The signal decays are fitted using a biexponential model with offset, which is necessary to account for incomplete conversions of the parent phases, (section S4) to extract the decay rates k_1 for the fast initial and k_2 for the slower regime for all investigated temperatures between 55°C and 90°C (for details compare SI section S4, Figures S21,S23-S24 and S26).[56] Still, the this way approximated decay rates k_1 and k_2 follow an Arrhenius type behaviour (Figure 3; dotted lines attributed to dominant decay rates). For a quantitative Arrhenius analysis, we focus on the decay rates and activation energies extracted from the XRD Arrhenius plots (Fig. 3C/D) and only qualitatively compare the results to NMR and PL. For both, NMR and PL spectroscopy, mixed perovskite phases also contribute to the observed signals and thus to the absolute values of the kinetic curves.

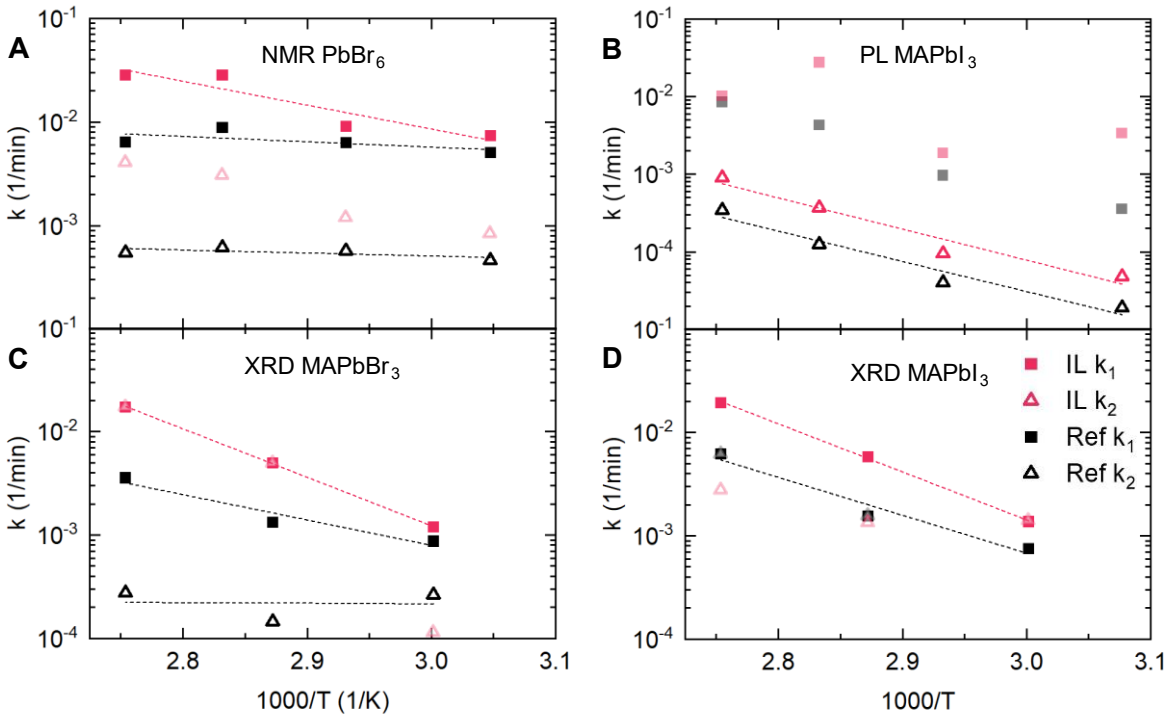

Figure 3: Arrhenius plot of decay rates k_1 and k_2 extracted from phase evolution of $MAPbBr_3$ and $MAPbI_3$ in a physical 1:1 mixture of $MAPbI_3$:$MAPbBr_3$ powder during thermally induced halide mixing with (IL) and without $BMIMBF_4$ (Ref). Decay rates extracted from the evolution of (A) $PbBr_6$ environments from ^{207}Pb NMR, (B) $MAPbI_3$ phase from PL, (C) $MAPbBr_3$ phase from XRD and (D) $MAPbI_3$ phase from XRD. The dashed lines are linear fits that yield the activation energy. They also indicate the rates with dominant (B,D) or equal (A,C) amplitude in saturated colors (see SI Section S4).

Comparing the behaviour of IL containing samples (red) and reference samples (black) within the Arrhenius plots (Figure 3) for all mixing temperatures and observation methods, we see that the extracted decay rates are up to an order-of-magnitude higher when the IL is present. In addition, it seems that the impact of the IL on the Br^- mixing rate (Figure 3A,3C) is more pronounced than for I^- (Figure 3B,3D). This results in nearly equal mixing rates for Br^- and I^- over a wide temperature range when the IL is present,

as demonstrated by a quantitative comparison of the I^- and Br^- rates extracted from XRD measurements (Figure 3 C,3D; solid red squares).

However, a stronger impact of $BMIMBF_4$ on Br^- diffusion is reflected in the slope of the linear Arrhenius fits of the dominant decay rates (dotted lines). For the IL containing sample, the slope associated with the fast decay rates k_1 of $MAPbBr_3$ increases significantly compared to the reference (solid squares, Figure 3A,C). The steeper slope transfers to a two-fold higher activation energy $E_{a,Br}$ for bromide migration, increasing from 47 to 90 kJ/mol as determined by the XRD measurement, when the IL is present (Table S6). Qualitatively, this trend of a significant increase in activation energies with IL is also observed in the NMR data for $PbBr_6$ environments (Table S6). The change of activation energy indicates that the IL $BMIMBF_4$ directly impacts on the mechanism of the mixing process, i.e., altering the nature of the Br^- diffusion pathway. As $BMIMBF_4$ coordinates to the perovskite interfaces,[43] it presumably changes the Br^- migration pathway at or between perovskite particle interfaces and grain boundaries.

In contrast, for $MAPbI_3$ only a negligible increase in slope is seen for the IL containing sample (solid squares, Figure 3B,3D). Consequently, the activation energies $E_{a,I}$ are not as strongly affected (Table S6) by the presence of IL, which are between 70 to 89 $kJmol^{-1}$ from XRD for reference and IL samples. The same trend is observed in the PL data following the dominant rates k_2 (Figure 3B, Table S6). As the magnitude of activation energies $E_{a,I}$ between reference and IL containing samples stay comparable, the nature of Iodide migration pathways are expected to be similar for both scenarios. However, the increase in I^- mixing rates when $BMIMBF_4$ is present (Figure 3B,3D) indicates that although the nature of diffusion pathways remains similar, the presence of IL increases their absolute number. This suggests an increase in accessible ionic defects at interfaces and/or the bulk.

In any case, the activation energies from XRD are between 47 and 90 $kJmol^{-1}$ for Br^- and between 70 to 89 $kJmol^{-1}$ for I^- migration, respectively, which is on average higher than the values known from literature.[22] Taking into account that literature values were measured either directly within thin film samples[11] or obtained with halide ion exchange between two thin films pressed together,[14] we propose that the looser contact between grains in our powder samples compared to thin films, elevates the average activation barrier. Still, the lower decay rates for Br^- compared to I^- despite a lower activation energy for Br^- seen for the reference samples is in accordance with literature investigating halide diffusion in perovskites in dark conditions.[21]

To gain a further insight into the behaviour of $BMIMBF_4$ at elevated temperatures, we conducted ^1H and ^{19}F MAS NMR experiments to probe the additive itself (Figure 4). The ^1H MAS NMR spectra of a $MAPbI_3/MAPbBr_3$ mixture with $BMIMBF_4$ at temperatures between 55°C and 90°C (Figure 4A) are dominated by the two signals of the ammonium ($-NH_3^+$) and the methyl group ($-CH_3$) of the methylammonium cation in the perovskite structure (for full spectra compare Figure S10). However, with increasing temperature, narrow ^1H signals corresponding to the imidazolium cation of the IL ($BMIM^+$) emerge (Figures 4A and S10).[59] At room temperature and up to 55°C, the ^1H MAS NMR signals are broad, as $BMIM^+$ coordinates to the perovskite surface resulting in a solid character[36] and passivates defect and trap states there[43]. The temperature-dependent narrowing of the $BMIM^+$ signals is due to a high increase in $BMIM^+$ mobility resulting in a liquid-like state (averaging of ^1H dipolar coupling terms) of the additive cations at high temperature. Hence, we conclude that the acceleration in the halide mixing process due to IL addition originates from the mobility of the IL cation $BMIM^+$: while at lower temperatures defects at grain boundaries and particle interfaces are efficiently saturated by the additive, the high $BMIM^+$ mobility at higher

temperatures opens these defect sites frequently, which are known to facilitate ion transport[15], and thus act as a 'highway' for halide diffusion for both, Iodide and Bromide.

Analogously, the BF_4^- anion is probed in the ^{19}F MAS NMR spectra, where we observe a clearly different behaviour for the neat parent samples containing $BMIMBF_4$: in the $MAPbBr_3$ powder the BF_4^- shows a liquid -like mobility with minor anisotropic interactions as probed by a single sharp ^{19}F resonance at -146.5 ppm. In contrast, the BF_4^- mobility is clearly reduced in $MAPbI_3$ powders, where the ^{19}F resonance at -149.0 ppm possesses spinning sidebands due to the presence of anisotropic interactions, and a broader linewidth. Both signatures indicate a stronger interaction between BF_4^- and the perovskite interface. Turning to a physical $MAPbI_3$/$MAPbBr_3$ mixture with $BMIMBF_4$ at room temperature both ^{19}F resonances are observed However, already before annealing the ratio between the sharp and the broader ^{19}F species is roughly 0.1:1, while at temperatures above of 45°C, and for emerging mixed halide $MAPbI_{3-x}Br_x$, only the broader resonance is visible (Figure 4B). This indicates that the highly mobile BF_4^- anions already diffuse to the $MAPbI_3$ powder grains at low temperatures and preferentially interact with the I-rich grain interfaces. In contrast to the $BMIM^+$ cation which gains mobility with higher temperatures, BF_4^- mobility shows only a small increase for increased temperatures up to 90°C as shown by a slight decrease in linewidth (Fig. S11). The accumulation of BF_4^- anions at I-rich interfaces might counteract the effect of the liberation of the $BMIM^+$ cations and thus mitigate the increase in Iodide migration.

However, we do not expect these mobility related effects of the additive ions to result in changes in activation energies, as the nature of the migration pathway is still defect-assisted. Rather an opening of interface defects via the liberation of $BMIM^+$ will lead to

a significant increase in mixing rates, while BF_4^- accumulation at Iodide rich-interfaces mitigates the effect for Iodide migration rates. Therefore, the increase in activation energy for Bromide migration upon presence of IL must be the result off another effect. Sanchora et al.[60] showed that in an imidazolium-based IL containing the super halogen BF_4^-, the imidazolium cation favors hydrogen bonding to halide ions in the order $Cl^->Br^->I^-$ instead of the super halogen. This implies that the $BMIM^+$ cation coordinates to halide ions and is shuttling these 'actively', further facilitating the halide transport between perovskite particles. In view that the interaction between $BMIM^+$ and Bromide is stronger than to Iodide,[60] this also explains the more pronounced acceleration in Br^- mixing rates (Figures 2 and 3 A,C) and the stronger influence on Bromide activation energies in comparison to Iodide with $BMIMBF_4$. Comparable shuttling mechanisms were already observed for imidazolium based ILs for applications as electrolytes in batteries: here the IL anions are forming complexes with Li^+ and are shuttling Li^+ cations between electrodes.[61]

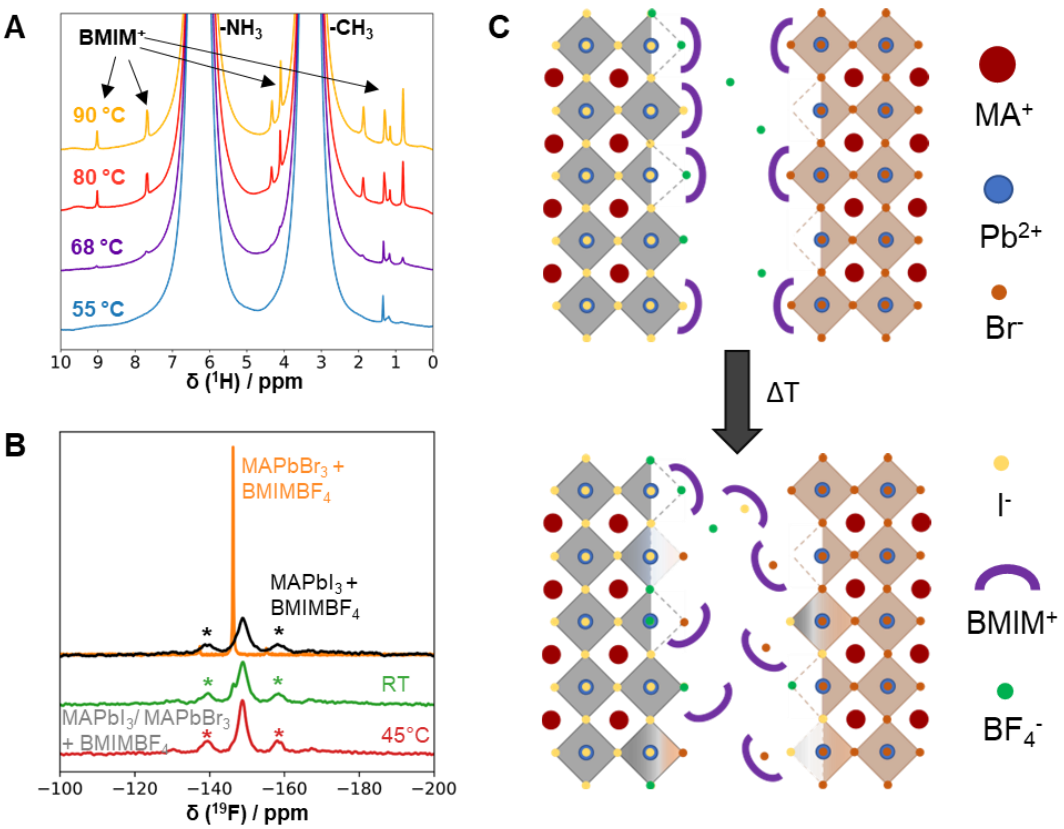

Figure 4: (A) ^{1}H MAS NMR spectra of the IL containing perovskite powder 1:1 mixture of $MAPbI_3$:$MAPbBr_3$ at various temperatures. The evolving resonances of $BMIMBF_4$ are labelled IL. (B) ^{19}F MAS NMR spectra of the IL containing perovskite powder 1:1 mixture of $MAPbI_3$:$MAPbBr_3$ prior annealing at RT (green) and at 45°C (red) compared to an overlay of normalized ^{19}F NMR spectra of $MAPbI_3$ with IL (black) and $MAPbBr_3$ with IL (orange). The resonances seen are associated to BF_4^- anions and spinning sidebands are marked with asterisks. (C) Proposed scheme of enhanced ion exchange for thermally induced halide mixing to form mixed halide perovskites. The scheme shows how $BMIMBF_4$ passivates trap states at grain boundaries and its mobility increase at elevated temperatures, while coordinating with halide ions.

In summary, the enhanced IL mobility with temperature opens defect-rich areas at grain boundaries and forms a liquid-like transfer channel of $BMIMBF_4$, where the

$BMIM^+$ cations may act as shuttles favoring Br^- transport, while accumulated BF_4^- anions at I-rich interfaces might partially counteract the effect of the liberation of the $BMIM^+$ cations. This interplay of coordinations results in an overall pronounced transport of halide ions to neighboring grains under dark conditions but favors Br^- migration. A sketch for the proposed mechanism of enhanced halide migration with $BMIMBF_4$ is shown in Figure 4C. We additionally investigated this proposed mechanism for another commonly used IL, $BMIMPF_6$, where compared to $BMIMBF_4$ the ionic radius of the anion PF_6^- is bigger (254 pm), hydrogen bonds between anion and cation are comparable[40] and the additive becomes in contrast to $BMIMBF_4$ hydrophobic.[62] We qualitatively observe a similar behaviour of accelerated halide kinetics at 90°C to form a solid solution from physical $MAPbI_3$/$MAPbBr_3$ powder mixtures containing $BMIMPF_6$ with overall comparable powder morphologies (see section S2 and S6). As we observe a similar trend for accelerated halide kinetics with $BMIMPF_6$, we conclude that our results are indicative of a more general behaviour. We propose that the addition of an IL with imidazolium-based cations, such as $BMIMBF_4$, known for their intrinsic ionic conductivity,[63,64] combined with a preferred interaction between the IL cation and Bromide and the IL anion and $MAPbI_3$ results in a more pronounced enhancement of Bromide migration rates compared to Iodide. Thus, the presence of the IL leads to an increase in the overall halide mixing rate, which is determined by the slowest halide migration rate.

This effect of $BMIMBF_4$ and $BMIMPF_6$ appears to be counter-intuitive to the literature, in which $BMIMBF_4$ was found to enhance the thermal stability in $MAPbI_3$ and mixed halide perovskite thin film solar cells under light irradiation and suppresses the ion migration in $MAPbI_3$ powder thick films under electrical bias.[36,42,43] Thus, we propose, that either equalized Iodide and Bromide migration rates decrease halide demixing

under illumination, or that the overall IL-enhanced halide mobility results in an equilibrium between halide demixing in excited regimes and remixing in dark parts. For many models of halide segregation under illumination, a difference in phase-segregation and mixing rates is a pre-requisite.[7,49,65,66] In future studies it will be promising to systematically address this proposed interplay between illumination and heat on the halide (de)mixing processes and associated kinetics under the influence of ionic conductors, such as ILs. Such studies will allow to identify suitable equilibrium conditions between halide mixing and demixing and consequently to develop stable mixed halide perovskite systems, fostering next-generation tandem solar cells.

Supporting Information

Experimental Details; Characterization of powder morphology of the parent powder educts $MAPbI_3$ and $MAPbBr_3$; In-situ experiments following the mixing process of $MAPbI_3$-$MAPbBr_3$; Kinetics of halide exchange from in-situ experiments; Activation energies for I and Br migration; Influence of the IL $BMIMPF_6$

Acknowledgements

The authors thank the DFG (Deutsche Forschungsgemeinschaft) for funding within project numbers 506642499 (SPP 2196/2), 492723217 (CRC 1585 MultiTrans), PA 3373/7-1 and MO 1060/32-1. H.G. thanks Prof. J. Senker and the Northern Bavarian NMR Centre (NBNC) for access to NMR and XRD machines, as well as Dr. Renée Siegel for support and discussions of NMR measurements. Further, H.G. thanks Prof. A.P.M Kentgens (Radboud University, Nijmegen) for scientific discussions and the PANACEA programme for supporting spectrometer access (European Union's Horizon 2020 research and innovation programme under Grant Agreement No 101008500). A.K., E.M.H. and C.G. are grateful to the "Bayrisches Staatsministerium für Unterricht und Kultus" for funding the project Solar Technologies go Hybrid (SolTech). We thank Tobias Siegert and Fatemeh Haddadi Barzoki for support with PL and NMR measurements.

References

(1) McMeekin, D. P.; Sadoughi, G.; Rehman, W.; Eperon, G. E.; Saliba, M.; Hörantner, M. T.; Haghighirad, A.; Sakai, N.; Korte, L.; Rech, B.; Johnston, M. B.; Herz, L. M.; Snaith, H. J. A mixed-cation lead mixed-halide perovskite absorber for tandem solar cells. *Science (New York, N.Y.)* **2016**, *351* (6269), 151–155.

(2) Xu, J.; Boyd, C. C.; Yu, Z. J.; Palmstrom, A. F.; Witter, D. J.; Larson, B. W.; France, R. M.; Werner, J.; Harvey, S. P.; Wolf, E. J.; Weigand, W.; Manzoor, S.; van Hest, M. F. A. M.; Berry, J. J.; Luther, J. M.; Holman, Z. C.; McGehee, M. D. Triple-halide wide-band gap perovskites with suppressed phase segregation for efficient tandems. *Science (New York, N.Y.)* **2020**, *367* (6482), 1097–1104.

(3) Hoke, E. T.; Slotcavage, D. J.; Dohner, E. R.; Bowring, A. R.; Karunadasa, H. I.; McGehee, M. D. Reversible photo-induced trap formation in mixed-halide hybrid perovskites for photovoltaics. *Chem. Sci.* **2015**, *6* (1), 613–617.

(4) Slotcavage, D. J.; Karunadasa, H. I.; McGehee, M. D. Light-Induced Phase Segregation in Halide-Perovskite Absorbers. *ACS Energy Lett.* **2016**, *1* (6), 1199–1205.

(5) Zhang, H.; Fu, X.; Tang, Y.; Wang, H.; Zhang, C.; Yu, W. W.; Wang, X.; Zhang, Y.; Xiao, M. Phase segregation due to ion migration in all-inorganic mixed-halide perovskite nanocrystals. *Nat. Commun.* **2019**, *10* (1), 1088.

(6) Motti, S. G.; Patel, J. B.; Oliver, R. D. J.; Snaith, H. J.; Johnston, M. B.; Herz, L. M. Phase segregation in mixed-halide perovskites affects charge-carrier dynamics while preserving mobility. *Nat. Commun.* **2021**, *12* (1), 6955.

(7) Yoon, S. J.; Kuno, M.; Kamat, P. V. Shift Happens . How Halide Ion Defects Influence Photoinduced Segregation in Mixed Halide Perovskites. *ACS Energy Lett.* **2017**, *2* (7), 1507–1514.

(8) Halford, G. C.; Deng, Q.; Gomez, A.; Green, T.; Mankoff, J. M.; Belisle, R. A. Structural Dynamics of Metal Halide Perovskites during Photoinduced Halide Segregation. *ACS Appl. Mater. Interfaces* **2022**, *14* (3), 4335–4343.

(9) Braly, I. L.; Stoddard, R. J.; Rajagopal, A.; Uhl, A. R.; Katahara, J. K.; Jen, A. K.-Y.; Hillhouse, H. W. Current-Induced Phase Segregation in Mixed Halide Hybrid Perovskites and its Impact on Two-Terminal Tandem Solar Cell Design. *ACS Energy Lett.* **2017**, *2* (8), 1841–1847.

(10) Lin, Y.; Chen, B.; Fang, Y.; Zhao, J.; Bao, C.; Yu, Z.; Deng, Y.; Rudd, P. N.; Yan, Y.; Yuan, Y.; Huang, J. Excess charge-carrier induced instability of hybrid perovskites. *Nat. Commun.* **2018**, *9* (1), 4981.

(11) Elmelund, T.; Seger, B.; Kuno, M.; Kamat, P. V. How Interplay between Photo and Thermal Activation Dictates Halide Ion Segregation in Mixed Halide Perovskites. *ACS Energy Lett.* **2020**, *5* (1), 56–63.

(12) Boukhvalov, D. W.; Zhidkov, I. S.; Akbulatov, A. F.; Kukharenko, A. I.; Cholakh, S. O.; Stevenson, K. J.; Troshin, P. A.; Kurmaev, E. Z. Thermal Effects and Halide Mixing of Hybrid Perovskites: MD and XPS Studies. *J. Phys. Chem. A* **2020**, *124* (1), 135–140.

(13) Wright, A. D.; Patel, J. B.; Johnston, M. B.; Herz, L. M. Temperature-Dependent Reversal of Phase Segregation in Mixed-Halide Perovskites. *Adv. Mater.* **2023**, e2210834.

(14) Elmelund, T.; Scheidt, R. A.; Seger, B.; Kamat, P. V. Bidirectional Halide Ion Exchange in Paired Lead Halide Perovskite Films with Thermal Activation. *ACS Energy Lett.* **2019**, *4* (8), 1961–1969.

(15) Lee, H.; Boonmongkolras, P.; Jun, S.; Kim, D.; Park, Y.; Koh, J.; Cho, Y.-H.; Shin, B.; Park, J. Y. In Situ Observation of Photoinduced Halide Segregation in Mixed Halide Perovskite. *ACS Appl. Energy Mater.* **2023**, *6* (3), 1565–1574.

(16) Barker, A. J.; Sadhanala, A.; Deschler, F.; Gandini, M.; Senanayak, S. P.; Pearce, P. M.; Mosconi, E.; Pearson, A. J.; Wu, Y.; Srimath Kandada, A. R.; Leijtens, T.; Angelis, F. de; Dutton, S. E.; Petrozza, A.; Friend, R. H. Defect-Assisted Photoinduced Halide Segregation in Mixed-Halide Perovskite Thin Films. *ACS Energy Lett.* **2017**, *2* (6), 1416–1424.

(17) Suchan, K.; Just, J.; Beblo, P.; Rehermann, C.; Merdasa, A.; Mainz, R.; Scheblykin, I. G.; Unger, E. Multi-Stage Phase-Segregation of Mixed Halide Perovskites under Illumination: A Quantitative

Comparison of Experimental Observations and Thermodynamic Models. *Adv. Funct. Mater.* **2023**, *33* (3), 2206047.
(18) Azpiroz, J. M.; Mosconi, E.; Bisquert, J.; Angelis, F. de. Defect migration in methylammonium lead iodide and its role in perovskite solar cell operation. *Energy Environ. Sci.* **2015**, *8* (7), 2118–2127.
(19) Li, C.; Guerrero, A.; Huettner, S.; Bisquert, J. Unravelling the role of vacancies in lead halide perovskite through electrical switching of photoluminescence. *Nat. Commun.* **2018**, *9* (1), 5113.
(20) Zhao, Y.; Miao, P.; Elia, J.; Hu, H.; Wang, X.; Heumueller, T.; Hou, Y.; Matt, G. J.; Osvet, A.; Chen, Y.-T.; Tarragó, M.; Ligny, D. de; Przybilla, T.; Denninger, P.; Will, J.; Zhang, J.; Tang, X.; Li, N.; He, C.; Pan, A.; Meixner, A. J.; Spiecker, E.; Zhang, D.; Brabec, C. J. Strain-activated light-induced halide segregation in mixed-halide perovskite solids. *Nat. Commun.* **2020**, *11* (1), 6328.
(21) McGovern, L.; Futscher, M. H.; Muscarella, L. A.; Ehrler, B. Understanding the Stability of MAPbBr3 versus MAPbI3: Suppression of Methylammonium Migration and Reduction of Halide Migration. *J. Phys. Chem. Lett.* **2020**, *11* (17), 7127–7132.
(22) Eames, C.; Frost, J. M.; Barnes, P. R. F.; O'Regan, B. C.; Walsh, A.; Islam, M. S. Ionic transport in hybrid lead iodide perovskite solar cells. *Nat. Commun.* **2015**, *6*, 7497.
(23) Tsai, H.; Asadpour, R.; Blancon, J.-C.; Stoumpos, C. C.; Durand, O.; Strzalka, J. W.; Chen, B.; Verduzco, R.; Ajayan, P. M.; Tretiak, S.; Even, J.; Alam, M. A.; Kanatzidis, M. G.; Nie, W.; Mohite, A. D. Light-induced lattice expansion leads to high-efficiency perovskite solar cells. *Science (New York, N.Y.)* **2018**, *360* (6384), 67–70.
(24) Bischak, C. G.; Hetherington, C. L.; Wu, H.; Aloni, S.; Ogletree, D. F.; Limmer, D. T.; Ginsberg, N. S. Origin of Reversible Photoinduced Phase Separation in Hybrid Perovskites. *Nano Lett.* **2017**, *17* (2), 1028–1033.
(25) Abdi-Jalebi, M.; Andaji-Garmaroudi, Z.; Cacovich, S.; Stavrakas, C.; Philippe, B.; Richter, J. M.; Alsari, M.; Booker, E. P.; Hutter, E. M.; Pearson, A. J.; Lilliu, S.; Savenije, T. J.; Rensmo, H.; Divitini, G.; Ducati, C.; Friend, R. H.; Stranks, S. D. Maximizing and stabilizing luminescence from halide perovskites with potassium passivation. *Nature* **2018**, *555* (7697), 497–501.
(26) Wang, Y.; Dar, M. I.; Ono, L. K.; Zhang, T.; Kan, M.; Li, Y.; Zhang, L.; Wang, X.; Yang, Y.; Gao, X.; Qi, Y.; Grätzel, M.; Zhao, Y. Thermodynamically stabilized β-CsPbI3-based perovskite solar cells with efficiencies 18. *Science (New York, N.Y.)* **2019**, *365* (6453), 591–595.
(27) Fu, Y.; Wu, T.; Wang, J.; Zhai, J.; Shearer, M. J.; Zhao, Y.; Hamers, R. J.; Kan, E.; Deng, K.; Zhu, X.-Y.; Jin, S. Stabilization of the Metastable Lead Iodide Perovskite Phase via Surface Functionalization. *Nano Lett.* **2017**, *17* (7), 4405–4414.
(28) Liu, D.; Shao, Z.; Gui, J.; Chen, M.; Liu, M.; Cui, G.; Pang, S.; Zhou, Y. A polar-hydrophobic ionic liquid induces grain growth and stabilization in halide perovskites. *Chem. Commun. (Cambridge, U. K.)* **2019**, *55* (74), 11059–11062.
(29) Wang, J.; Ye, X.; Wang, Y.; Wang, Z.; Wong, W.; Li, C. Halide perovskite based on hydrophobic ionic liquid for stability improving and its application in high-efficient photovoltaic cell. *Electrochim. Acta* **2019**, *303*, 133–139.
(30) Chen, P.; Zhang, Y.; Du, J.; Wang, Y.; Zhang, X.; Liu, Y. Global Control of CH 3 NH 3 PbI 3 Formation with Multifunctional Ionic Liquid for Perovskite Hybrid Photovoltaics. *J. Phys. Chem. C* **2018**, *122* (20), 10699–10705.
(31) Wan, Y.; Dong, S.; Wang, Y.; Yang, L.; Qin, W.; Cao, H.; Yao, C.; Ge, Z.; Yin, S. Ionic liquid-assisted perovskite crystal film growth for high performance planar heterojunction perovskite solar cells. *RSC Adv.* **2016**, *6* (100), 97848–97852.
(32) Gu, L.; Ran, C.; Chao, L.; Bao, Y.; Hui, W.; Wang, Y.; Chen, Y.; Gao, X.; Song, L. Designing Ionic Liquids as the Solvent for Efficient and Stable Perovskite Solar Cells. *ACS Appl. Mater. Interfaces* **2022**, 14 (20), 22870–22878.

(33) Chu, W.; Yang, J.; Jiang, Q.; Li, X.; Xin, J. Enhancement of photovoltaic performance of flexible perovskite solar cells by means of ionic liquid interface modification in a low temperature all solution process. *Appl. Surf. Sci.* **2018**, *440*, 1116–1122.
(34) Li, M.; Zhao, C.; Wang, Z.-K.; Zhang, C.-C.; Lee, H. K. H.; Pockett, A.; Barbé, J.; Tsoi, W. C.; Yang, Y.-G.; Carnie, M. J.; Gao, X.-Y.; Yang, W.-X.; Durrant, J. R.; Liao, L.-S.; Jain, S. M. Interface Modification by Ionic Liquid: A Promising Candidate for Indoor Light Harvesting and Stability Improvement of Planar Perovskite Solar Cells. *Adv. Energy Mater.* **2018**, *8* (24), 1801509.
(35) Huang, X.; Guo, H.; Wang, K.; Liu, X. Ionic liquid induced surface trap-state passivation for efficient perovskite hybrid solar cells. *Org. Electron.* **2017**, *41*, 42–48.
(36) Ramming, P.; Leupold, N.; Schötz, K.; Köhler, A.; Moos, R.; Grüninger, H.; Panzer, F. Suppressed ion migration in powder-based perovskite thick films using an ionic liquid. *J. Mater. Chem. C* **2021**, *9* (35), 11827–11837.
(37) Du, Y.; Tian, Q.; Chang, X.; Fang, J.; Gu, X.; He, X.; Ren, X.; Zhao, K.; Liu, S. F. Ionic Liquid Treatment for Highest-Efficiency Ambient Printed Stable All-Inorganic CsPbI3 Perovskite Solar Cells. *Adv. Mater.* **2022**, *34* (10), e2106750.
(38) Xu, J.; Cui, J.; Yang, S.; Han, Y.; Guo, X.; Che, Y.; Xu, D.; Duan, C.; Zhao, W.; Guo, K.; Ma, W.; Xu, B.; Yao, J.; Liu, Z.; Liu, S. Unraveling Passivation Mechanism of Imidazolium-Based Ionic Liquids on Inorganic Perovskite to Achieve Near-Record-Efficiency CsPbI2Br Solar Cells. *Nano-Micro Lett.* **2021**, *14* (1), 7.
(39) Ban, H.; Zhang, Z.; Dai, L.; Liu, Z.; Yu, H.; Shen, Y.; Zhang, X.-L.; Zhu, J.; Wang, M. Efficient and Stable Mesoporous CsSnI 3 Perovskite Solar Cells via Imidazolium-Based Ionic Liquid Additive. *Sol. RRL* **2022**, *6* (12), 2200827.
(40) Dong, K.; Song, Y.; Liu, X.; Cheng, W.; Yao, X.; Zhang, S. Understanding structures and hydrogen bonds of ionic liquids at the electronic level. *J. Phys. Chem. B* **2012**, *116* (3), 1007–1017.
(41) Wang, Y.; Yang, Y.; Li, N.; Hu, M.; Raga, S. R.; Jiang, Y.; Wang, C.; Zhang, X.-L.; Lira-Cantu, M.; Huang, F.; Cheng, Y.-B.; Lu, J. Ionic Liquid Stabilized Perovskite Solar Modules with Power Conversion Efficiency Exceeding 20%. *Adv. Funct. Mater.* **2022**, *32* (38).
(42) Zheng, X.; Jiang, T.; Bai, L.; Chen, X.; Chen, Z.; Xu, X.; Song, D.; Xu, X.; Li, B.; Yang, Y. M. Enhanced thermal stability of inverted perovskite solar cells by interface modification and additive strategy. *RSC Adv.* **2020**, *10* (31), 18400–18406.
(43) Bai, S.; Da, P.; Li, C.; Wang, Z.; Yuan, Z.; Fu, F.; Kawecki, M.; Liu, X.; Sakai, N.; Wang, J. T.-W.; Huettner, S.; Buecheler, S.; Fahlman, M.; Gao, F.; Snaith, H. J. Planar perovskite solar cells with long-term stability using ionic liquid additives. *Nature* **2019**, *571* (7764), 245–250.
(44) Kim, H.; Lim, J.; Sohail, M.; Nazeeruddin, M. K. Superhalogen Passivation for Efficient and Stable Perovskite Solar Cells. *Sol. RRL* **2022**, *6* (7), 2200013.
(45) Leupold, N.; Schötz, K.; Cacovich, S.; Bauer, I.; Schultz, M.; Daubinger, M.; Kaiser, L.; Rebai, A.; Rousset, J.; Köhler, A.; Schulz, P.; Moos, R.; Panzer, F. High Versatility and Stability of Mechanochemically Synthesized Halide Perovskite Powders for Optoelectronic Devices. *ACS Appl. Mater. Interfaces* **2019**, *11* (33), 30259–30268.
(46) Yin, R.; Wang, K.-X.; Cui, S.; Fan, B.-B.; Liu, J.-W.; Gao, Y.-K.; You, T.-T.; Yin, P.-G. Dual-Interface Modification with BMIMPF 6 for High-Efficiency and Stable Carbon-Based CsPbI 2 Br Perovskite Solar Cells. *ACS Appl. Energy Mater.* **2021**, *4* (9), 9294–9303.
(47) McGovern, L.; Koschany, I.; Grimaldi, G.; Muscarella, L. A.; Ehrler, B. Grain Size Influences Activation Energy and Migration Pathways in MAPbBr3 Perovskite Solar Cells. *J. Phys. Chem. Lett.* **2021**, *12* (9), 2423–2428.
(48) Fykouras, K.; Lahnsteiner, J.; Leupold, N.; Tinnemans, P.; Moos, R.; Panzer, F.; Wijs, G. A. de; Bokdam, M.; Grüninger, H.; Kentgens, A. P. M. Disorder to order: how halide mixing in MAPbI 3− x Br x perovskites restricts MA dynamics. *J. Mater. Chem. A* **2023**, *11* (9), 4587–4597.

(49) Draguta, S.; Sharia, O.; Yoon, S. J.; Brennan, M. C.; Morozov, Y. V.; Manser, J. S.; Kamat, P. V.; Schneider, W. F.; Kuno, M. Rationalizing the light-induced phase separation of mixed halide organic-inorganic perovskites. *Nat. Commun.* **2017**, *8* (1), 200.
(50) Franssen, W. M. J.; van Es, S. G. D.; Dervişoğlu, R.; Wijs, G. A. de; Kentgens, A. P. M. Symmetry, Dynamics, and Defects in Methylammonium Lead Halide Perovskites. *J. Phys. Chem. Lett.* **2017**, *8* (1), 61–66.
(51) Karmakar, A.; Askar, A. M.; Bernard, G. M.; Terskikh, V. V.; Ha, M.; Patel, S.; Shankar, K.; Michaelis, V. K. Mechanochemical Synthesis of Methylammonium Lead Mixed–Halide Perovskites: Unraveling the Solid-Solution Behavior Using Solid-State NMR. *Chem. Mater.* **2018**, *30* (7), 2309–2321.
(52) Knight, A. J.; Wright, A. D.; Patel, J. B.; McMeekin, D. P.; Snaith, H. J.; Johnston, M. B.; Herz, L. M. Electronic Traps and Phase Segregation in Lead Mixed-Halide Perovskite. *ACS Energy Lett.* **2019**, *4* (1), 75–84.
(53) Noh, J. H.; Im, S. H.; Heo, J. H.; Mandal, T. N.; Seok, S. I. Chemical management for colorful, efficient, and stable inorganic-organic hybrid nanostructured solar cells. *Nano Lett.* **2013**, *13* (4), 1764–1769.
(54) Sutter-Fella, C. M.; Li, Y.; Amani, M.; Ager, J. W.; Toma, F. M.; Yablonovitch, E.; Sharp, I. D.; Javey, A. High Photoluminescence Quantum Yield in Band Gap Tunable Bromide Containing Mixed Halide Perovskites. *Nano Lett.* **2016**, *16* (1), 800–806.
(55) Nakamura, Y.; Shibayama, N.; Hori, A.; Matsushita, T.; Segawa, H.; Kondo, T. Crystal Systems and Lattice Parameters of CH3NH3Pb(I1-xBrx)3 Determined Using Single Crystals: Validity of Vegard's Law. *Inorg. Chem.* **2020**, *59* (10), 6709–6716.
(56) Atkins, P.; Paula, J. de. *Thermodynamics and kinetics*, 8th ed.; Physical chemistry, v. 1; W.H. Freeman and Co, 2005.
(57) Belisle, R. A.; Bush, K. A.; Bertoluzzi, L.; Gold-Parker, A.; Toney, M. F.; McGehee, M. D. Impact of Surfaces on Photoinduced Halide Segregation in Mixed-Halide Perovskites. *ACS Energy Lett.* **2018**, *3* (11), 2694–2700.
(58) McGovern, L.; Grimaldi, G.; Futscher, M. H.; Hutter, E. M.; Muscarella, L. A.; Schmidt, M. C.; Ehrler, B. Reduced Barrier for Ion Migration in Mixed-Halide Perovskites. *ACS Appl. Energy Mater.* **2021**, *4* (12), 13431–13437.
(59) Biberger, S.; Schötz, K.; Ramming, P.; Leupold, N.; Moos, R.; Köhler, A.; Grüninger, H.; Panzer, F. How the ionic liquid BMIMBF 4 influences the formation and optoelectronic properties of MAPbI 3 thin films. *J. Mater. Chem. A* **2022**, *10* (35), 18038–18049.
(60) Sanchora, P.; Pandey, D. K.; Rana, D.; Materny, A.; Singh, D. K. Impact of Size and Electronegativity of Halide Anions on Hydrogen Bonds and Properties of 1-Ethyl-3-methylimidazolium-Based Ionic Liquids. *J. Phys. Chem. A* **2019**, *123* (23), 4948–4963.
(61) Gouverneur, M.; Schmidt, F.; Schönhoff, M. Negative effective Li transference numbers in Li salt/ionic liquid mixtures: does Li drift in the "Wrong" direction? *Phys. Chem. Chem. Phys. P* **2018**, *20* (11), 7470–7478.
(62) Del Valle, J. C.; García Blanco, F.; Catalán, J. Empirical parameters for solvent acidity, basicity, dipolarity, and polarizability of the ionic liquids BMIMBF4 and BMIMPF6. *J. Phys. Chem. B* **2015**, *119* (13), 4683–4692.
(63) Navarra, M. A. Ionic liquids as safe electrolyte components for Li-metal and Li-ion batteries. *MRS Bull.* **2013**, *38* (7), 548–553.
(64) MacFarlane, D. R.; Tachikawa, N.; Forsyth, M.; Pringle, J. M.; Howlett, P. C.; Elliott, G. D.; Davis, J. H.; Watanabe, M.; Simon, P.; Angell, C. A. Energy applications of ionic liquids. *Energy Environ. Sci.* **2014**, *7* (1), 232–250.

(65) Ruth, A.; Brennan, M. C.; Draguta, S.; Morozov, Y. V.; Zhukovskyi, M.; Janko, B.; Zapol, P.; Kuno, M. Vacancy-Mediated Anion Photosegregation Kinetics in Mixed Halide Hybrid Perovskites: Coupled Kinetic Monte Carlo and Optical Measurements. *ACS Energy Lett.* **2018**, *3* (10), 2321–2328.
(66) Chen, Z.; Brocks, G.; Tao, S.; Bobbert, P. A. Unified theory for light-induced halide segregation in mixed halide perovskites. *Nat. Commun.* **2021**, *12* (1), 2687.